Propagation and Growth of Gulf Stream Meanders between 75° and 45°W

TONG LEE

Department of Earth, Atmospheric, and Planetary Sciences, Massachusetts Institute of Technology, Cambridge, Massachusetts

PETER CORNILLON

Graduate School of Oceanography, University of Rhode Island, Narragansett, Rhode Island

(Manuscript received 29 March 1994, in final form 25 July 1995)

ABSTRACT

Analysis of the Gulf Stream path between 75° and 60°W indicates that the spectral signature of propagating and standing meanders is qualitatively similar to that observed for the upstream region 74°–70°W. Progressive, retrogressive, and standing meanders coexist at periods of several months and longer.

The amplitude-dependent dispersion relation obtained for the region 75°–45°W demonstrates the decrease of phase speed as the amplitude increases; the dependence of phase speed on amplitude is found to be stronger than that on wavelength. The average phase speed decreases with downstream distance primarily due to the downstream increase of meander amplitude. Consequently, a relation between phase speed and wavelength for the region west of 70°W, averaged over all amplitudes, is not uniformly valid for a larger domain. Furthermore, downstream propagating meander troughs are steeper and travel more slowly than meander crests. The average stationary wavelength, 700–800 km for 75°–60°W, is much shorter than that predicted based on an equivalent barotropic, β-plane thin-jet model.

The most energetic meanders have a period of 46 days and a wavelength of 427 km. The period of the fastest-growing meanders is approximately 40 days, close to the period of the most energetic meanders. The wavelength of the fastest-growing meanders, about 350 km, is shorter than the wavelength of the most energetic meanders.

The New England Seamounts do not have a significant effect on the most energetic meanders. However, meanders having periods either shorter or longer than the period of the most energetic meanders are affected by the seamounts. For long-period meanders, their lateral excursions seem to be constrained by the seamounts.

1. Introduction

Over the past 20 years there have been a number of analyses of different datasets to characterize the propagation and growth of Gulf Stream meanders (Hansen and Maul 1970; Maul et al. 1978; Halliwell and Mooers 1979, 1983; Watts and Johns 1982; Kontoyiannis and Watts 1994). Despite these studies, the picture that emerges today is still quite incomplete. Furthermore, a robust comparison of meander statistics with predictions by theories and numerical models has not been done. As part of the SYNOP (Synoptic Ocean Prediction) program, a study was undertaken to fill in some of the gaps in this picture using 8 years (1982–1989) of satellite infrared data. The goal of the study is to extend the observational scope of the path variability of the Gulf Stream in the space–time continuum and to investigate the underlying physics. Three manuscripts, of which this is the second, have resulted from this work. The first, Lee and Cornillon (1996), describes three methods used to determine the dispersion relation of Gulf Stream meanders from satellite-derived paths of the Gulf Stream. The analyses were confined to the region between 74° and 70°W; this region was also sampled by Inverted Echo Sounders, thus allowing for a comparison of the dispersion relation obtained from in situ data with that derived from the satellite data. The results of this comparison show that the dispersion relation derived from satellite data is consistent with that obtained from in situ data for short-period meanders. In addition, a number of properties of meanders in this region were quantified. In particular, progressive (downstream propagating) and retrogressive (upstream propagating) meanders are found to coexist at periods longer than several months, and they are delimited in wavelength by stationary meanders 1100 km long. The phase speed is a function of amplitude as well as wavelength. Planetary β, vortex induction, and advection, identified by Cushman-Roision et al. (1993) to be factors controlling meander propagation, all appear to contribute to the phase speed. The topographic β effect may also be important in this region. This, the second manuscript, focuses on the propagation and growth of meanders from the point at which the Gulf

Corresponding author address: Dr. Tong Lee, Dept. of Earth, Atmospheric, and Planetary Sciences, Center for Meteorology and Physical Oceanography, Massachusetts Institute of Technology, Cambridge, MA 02139.

Stream separates from the continental shelf (75°W) to the point at which it bifurcates into a recirculation branch and the North Atlantic Current (45°W), a much larger geographic region than analyzed for Lee and Cornillon (1996).

The third manuscript (Lee and Cornillon, 1995) deals with long-period (seasonal to interannual) fluctuations in the path's spatial root-mean-square variability due to meandering and with large-scale lateral oscillations of the path that are nonmeandering in nature.

The first issue addressed in this manuscript (section 3) is the most energetic time and length scales of propagating meanders. We first demonstrate that these meanders are energetic over a broad space–time continuum. The period and wavelength of the most energetic propagating meanders are then quantified. From this, we show that the most energetic wavelength is longer than previously thought.

The second issue addressed relates to the propagation characteristics of meanders. The phase speeds observed by Hansen (1970) and Halliwell and Mooers (1983) between 75° and 60°W are much smaller than those observed upstream of 70°W by Watts and Johns (1982) or by Kontoyiannis and Watts (1994). Consistent with these observations, Gilman (1986) found that the average phase speed of meanders tends to decrease and the average amplitude increases with downstream distance. Given these observations, one is naturally led to ask whether the downstream decrease of phase speed is due to the downstream increase in amplitude or to changes in stream structure and topography. Or, more significantly, does the dispersion relation change with downstream distance? In section 4, the strong dependence of phase speed on amplitude is discussed. We then show that this amplitude dependence is the major cause for the downstream decrease of phase speed and that an amplitude-averaged dispersion relation derived from data upstream of 70°W is not uniformly valid over a larger domain.

The third issue addressed relates to the growth of meanders. Gulf Stream meanders are commonly viewed as unstable disturbances that extract available potential energy and/or kinetic energy from the mean flow via baroclinic and/or barotropic instabilities. Previous studies of meander growth are either confined within small upstream regions (Watts and Johns 1982; Kontoyiannis and Watts 1994), limited to a specific wavelength (Halliwell and Mooers 1983), or based on a limited number of path realizations collected through shipboard surveys (Hansen 1970; Robinson et al. 1974). Consequently, the knowledge of meander growth has been very limited. Furthermore, all observed growth rates are spatial growth rates, while models and theories usually predict temporal growth rates. This poses a problem when model–data comparisons are undertaken. In section 5, the spatial and the temporal growth of meanders for various periods and wavelengths are quantified independently, scales of the fastest-growing meanders are determined and compared with model predictions, and the relation between the spatial and temporal growth rates is examined.

Observations of Cornillon and Boman (1987) suggest that meander crests that detached to form warm core rings traveled significantly more slowly than troughs that detached to form cold core rings. Apart from this, little work has been done to examine differences between meander crest and trough propagation characteristics. In section 6, individual measurements of crests and troughs are analyzed separately. We found that the propagation and growth characteristics of crests and troughs are indeed different. A possible cause of the crest–trough differences is discussed.

Finally, the effect of the New England Seamounts on Gulf Stream meanders is investigated. There has been conflicting evidence as to how the seamounts affect the Gulf Stream. Some studies (Richardson 1981; Teague and Hallock 1990) suggest a significant increase of meander amplitudes when the stream crosses the seamount chain; others (Cornillon 1986; Auer 1987) indicate that there is no significant change in the envelope of meandering paths across the seamounts. In section 7, spatial structures of meanders for various frequency bands are investigated. The results explain why there has been a controversy with regard to the effect of the seamounts.

A brief description of the data and methodology is provided in section 2. Results of the analysis related to the aforementioned issues are presented in sections 3–7. The findings are summarized in section 8.

2. Data and methodology

This study relies on positions of the Gulf Stream path digitized from AVHRR-derived infrared images of sea surface temperature for the period April 1982–December 1989. The study domain extends from 75° to 45°W. Details of the processing required to obtain sea surface temperature (SST) fields from satellite-derived infrared data and the procedure used to digitize the path of the Gulf Stream from the SST fields are described in Cornillon et al. (1987) and in Lee and Cornillon (1996).

Four different approaches were taken toward the analysis of these paths. The first three methods are all space–time analyses and thus require complete paths. Because of the dramatic increase in cloud cover that often obscures the stream for extended periods east of approximately 60°W, the study area to which these analyses are applied is restricted to the region from 75° to 60°W. For this region, a set of space–time displacements of the stream path is obtained by the following procedure: 1) each path, defined by a sequence of positions, is transformed to a coordinate system with the x axis parallel to the portion of the mean path between

75° and 60°W for the entire study period. The origin of the new coordinate system is located at (75°W, 35.5°N), and the x axis is 18° north of east; 2) multivalued path segments are modified to yield single-valued segments; and 3) spline interpolation in space and time is applied to the single-valued paths. The splines are sampled every 20 km in space and 2 days in time. The resultant space–time data matrix of path displacements, consisting of 66 time series at equally spaced locations, is the basis for the three space–time analyses. The fourth method, analysis of individual meanders, does not require a continuous series of Gulf Stream paths. For this reason, a measure of meander characteristics for the entire domain from 75° to 45°W is possible. The four analysis methods, discussed in detail in Lee and Cornillon (1996), are briefly summarized below.

The first method is the analysis of the wavenumber–frequency spectrum. For a space–time dataset, each time series is first transformed into complex coefficients corresponding to different frequency harmonics by the fast Fourier transform. The wavenumber spectrum at each frequency is then obtained by applying autoregressive (AR) modeling to the complex coefficients corresponding to that frequency but different spatial locations. The parametric assumption of the AR model provides for high resolution in wavenumber and allows for estimates of lengthscales that are larger than the width of the study area.

The second approach is the analysis of real empirical orthogonal functions (EOF) in the time domain. This is accomplished by decomposing the covariance matrix of the space–time data into mutually orthogonal eigenmodes. Each mode is associated with an eigenvalue reflecting the variance explained by this mode, an empirical orthogonal function describing the spatial structure of a coherent fluctuation, and a time series (principal component) illustrating the temporal variation of this spatial structure.

In the third approach, analysis of complex empirical orthogonal functions (CEOF) in the frequency domain, the covariance matrix of the EOF analysis is replaced by the cross-spectral matrix of a frequency band of interest; phase information, not preserved in the covariance matrix of the EOF analysis, is thus contained in the cross-spectral matrix of the CEOF analysis.

The last method measures properties of meander crests and troughs directly from the digitized paths using an objective algorithm (also described in detail in Cornillon et al. 1994). The algorithm only resolves meanders having wavelengths from about 200 to 800 km. Short path segments and highly convoluted segments are excluded by the algorithm. For an observation of a meander at a given time, the method provides a measurement of the center location, wavelength, amplitude, phase speed, and temporal growth rate. To reduce the statistical correlation of observations corresponding to the same meander, these observations are grouped into nonoverlapping 10-day segments (the approximate decorrelation timescale), and the averaged wavelength, amplitude, phase speed, and temporal growth rate are obtained for each segment. In the following, discussion of the properties of individually measured meanders, in fact, refers to these 10-day-averaged quantities.

3. Types of meanders and scales of the most energetic propagating meanders

In this section, we first demonstrate the presence of propagating and standing meanders in the study area through analyses of wavenumber–frequency spectra and of EOFs. The period and wavelength of the most energetic propagating meanders are then determined from the propagating wavenumber–frequency spectrum and compared with previous observations.

The wavenumber–frequency spectrum of the space–time path displacements between 75° and 60°W is calculated. The full spectrum $S(\pm k, f)$, the propagating spectrum $PR(k, f) = S(k, f) - S(-k, f)$, and the standing spectrum $ST(k, f) = \min[S(k, f), S(-k, f)]$, computed with an order-12 AR model, are shown in Figs. 1a–c [a detailed discussion of these spectral components is provided in Lee and Cornillon (1996)]. The propagating spectrum (Fig. 1b) is similar to that for the upstream region (74°–70°W) studied in Lee and Cornillon (1996): a positive ridge extending over a large part of the frequency range is associated with progressive meanders; a small pool of negative spectral densities at low frequencies and small wavenumbers (dashed contours) indicating the coexistence of retrogressive meanders with progressive ones. The standing spectrum (Fig. 1c) also resembles that of the upstream area, with large spectral densities at low frequency and small wavenumber where oppositely traveling waves coexist, suggesting the presence of standing waves. These spectral features are robust over a wide range of AR model orders from 6 to over 26. In general, lower-order AR models tend to produce overly smoothed spectra, while higher-order ones may result in spurious spikes. The robustness of these results over such a wide range of orders is therefore significant. We also compared these spectra with those computed by two-dimensional FFT. The distributions of propagating and standing variance for the two types of spectra are similar. This again suggests that the use of high-resolution AR modeling is appropriate. To illustrate the statistical significance of the spectra, Monte Carlo simulations were performed based on 100 sets of 2D random data. Figure 2 presents the ratio of absolute spectral density of the actual data to the 95% confidence intervals derived from the simulations. The progressive ridge is seen to be significant to a period of about 8 days (contour level > 1.0). The low-frequency, small-wavenumber retrogressive variance and standing variance are also significant.

The full and propagating spectra presented in Fig. 1 are compared with those computed by Halliwell and

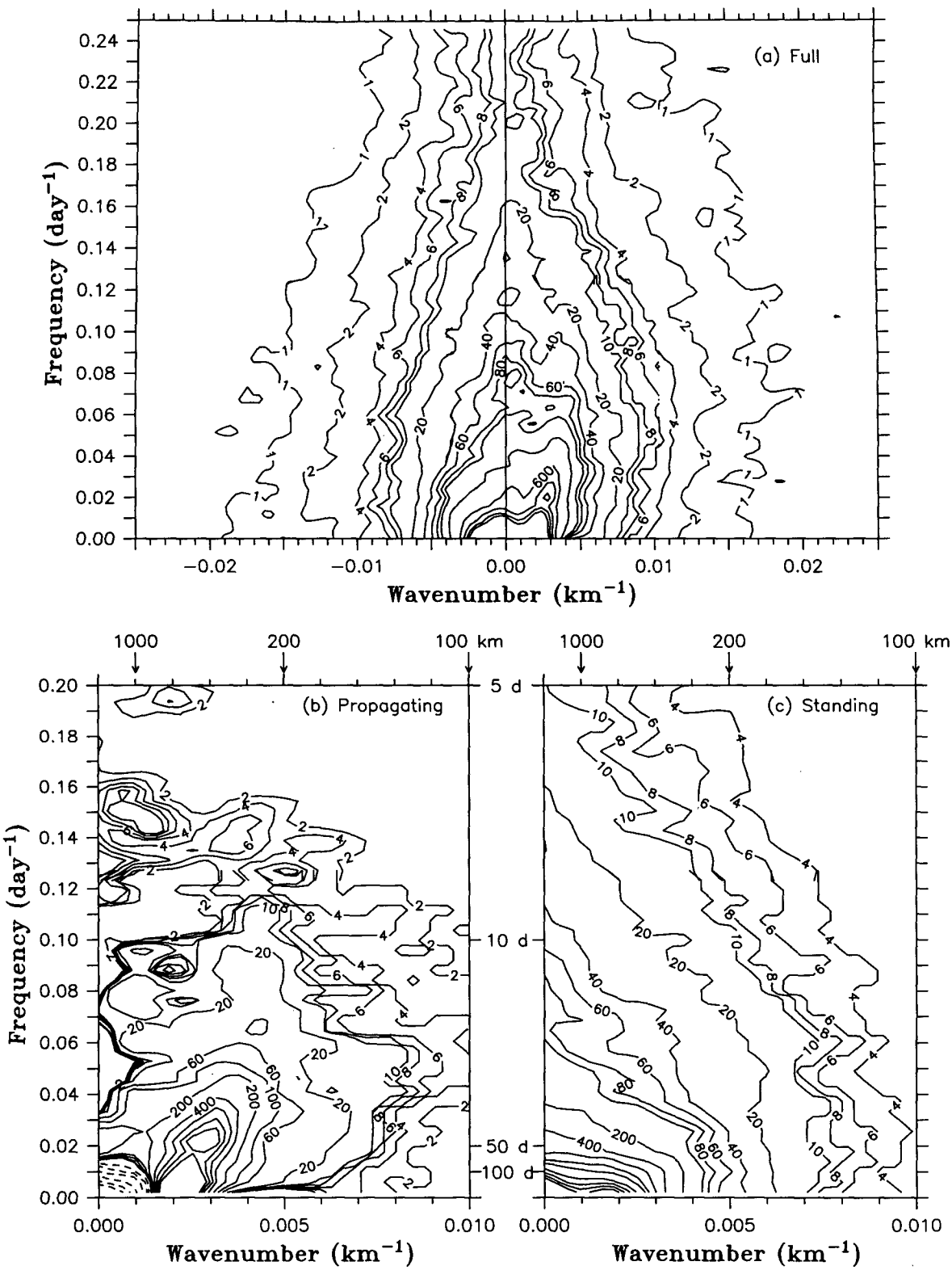

FIG. 1. Wavenumber–frequency spectra of the Gulf Stream path: (a) full spectrum, (b) propagating spectrum, and (c) standing spectrum. Contour levels indicate spectral density $\times 10^{-3}$ (km^2 $\times$ day^{-1} km^{-1}). In (b) levels of dashed contours are -250, -500, -1000, -2000, -3000, and -4000 toward zero frequency.

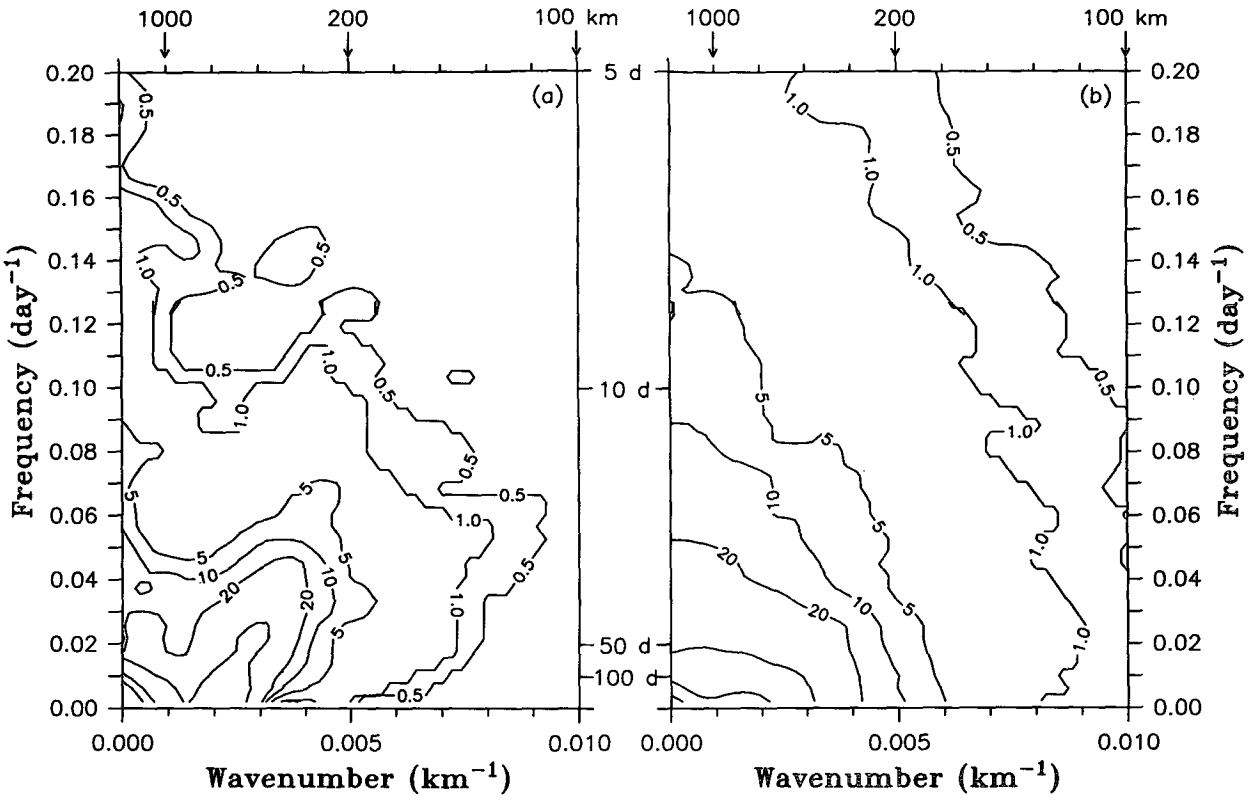

FIG. 2. Ratio of the absolute spectral density to the 95% confidence interval for (a) propagating spectrum and (b) standing spectrum.

Mooers (1983) reproduced in Fig. 3. The latter are based on path displacements between 73° and 65°W digitized from the NOAA frontal charts prepared from weekly composite infrared images for the period of 1975–1978. The positive ridge associated with progressive meanders is seen in both spectra. In the Halliwell and Mooers propagating spectrum, there is a large pool of negative spectral density for frequencies of 18–26 yr^{-1} corresponding to 0.05–0.07 day^{-1} (periods of 20–14 days) in the units of our spectrum. Halliwell and Mooers stated that their spectral estimates at these frequencies are relatively unreliable because of the large sampling interval (7 days). We do not observe negative spectral density at these frequencies.

The ensemble-averaged propagating frequency spectrum and wavenumber spectrum are obtained from the propagating FFT-AR wavenumber–frequency spectrum (Fig. 1b). This is done by averaging the wavenumber spectrum over frequency and the frequency spectrum over wavenumber. The results are shown in Fig. 4. The most energetic period determined from the peak frequency (Fig. 4a) is 46 ± 8 days (the uncertainty is at the 95% confidence level), which agrees with that reported by Halliwell and Mooers (1983), 1.5 months. The most energetic wavelength determined from the peak wavenumber (solid curve in Fig. 4b) is 427 km for this order-12 AR model. (The mean of the peak wavelength over model orders 6–24 is 425 km with a standard error of 16 km.) The most energetic wavelength is not biased by the use of the AR model; the 2D-FFT propagating spectrum also yields a most energetic wavelength of 427 ± 70 km.

Halliwell and Mooers (1983) reported that the most energetic wavelength was 330 km. However, their "most energetic" wavelength, also determined from the propagating wavenumber spectrum, is defined as the wavelength for which half of the propagating variance exists at longer wavelengths. The reason that they defined it this way was because their spectrum had low wavenumber resolution and a flat peak. We refer to this wavelength as the mean wavelength because it is actually a measure of the average wavelength rather than the most energetic one. The two are different for a skewed spectrum. The mean wavelength determined from our data is 394 km both for the AR- and FFT-derived spectra. This is slightly shorter than the most energetic wavelength, but still longer than that reported by Halliwell and Mooers. Our data, reanalyzed for the region used by Halliwell and Mooers (73°–65°W), yields the same result as for the entire region. Therefore, neither the difference in measure (mean/most energetic), period (1975–1978/1982–1989), nor region

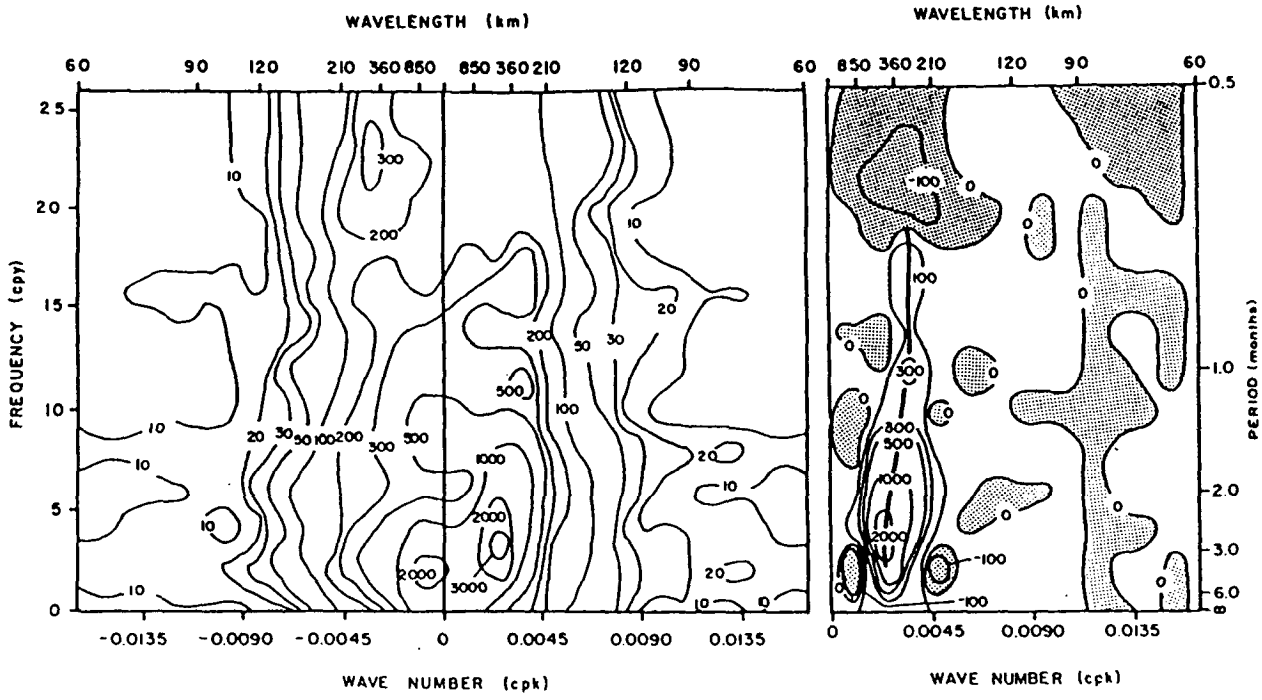

FIG. 3. Wavenumber–frequency spectra of propagating meander time series (73°–65°W) computed by Halliwell and Mooers (1983). (Left) full spectrum, (right) propagating spectrum. Contours are in km^2 week^{-1} km^{-1} × 10^{-3}.

(73–65°W/75–60°W) explains the difference between the Halliwell and Mooers observation of the most energetic meanders and ours.

An alternative explanation relates to the method used to process the data. Halliwell and Mooers (1983) decomposed their raw space–time data into orthogonal modes by EOF analysis, then reconstructed a "propagating" space–time dataset by dropping modes that they believed to be associated with standing waves and noise. However, in Lee and Cornillon (1996), it was found that some propagating long meanders are correlated with standing meanders. Consequently, a mode that is the most representative of the actual standing waves may contain some propagating variance. Halliwell and Mooers (1983) excluded their mode 4, which is representative of coherent standing meanders. This may have in fact removed some variance of long, propagating meanders. As a result, spectral densities at longer wavelengths (small wavenumbers) would decrease, resulting in a shift of the spectral peak to a shorter wavelength (larger wavenumber).

To verify this speculation, we reanalyze our data using the approach taken by Halliwell and Mooers (1983). First, we obtain 66 eigenmodes through EOF analysis. The second EOF (Fig. 5a) (explaining 18% of the total variance) reveals a standing wave pattern similar to the Halliwell and Mooers mode 4. The frequency autospectrum of the principal component time series of this mode (Fig. 5b) indicates that this mode is energetic at periods longer than several months, which is also similar to the Halliwell and Mooers mode 4. Given this similarity, we reconstructed a new data matrix by excluding this mode. The propagating wavenumber spectrum computed from the new data matrix is presented in Fig. 4 (dotted curve). Compared to the original spectrum (solid curve), the peak of the new spectrum is seen to shift toward smaller wavelengths. The most energetic wavelength and the mean wavelength determined from this spectrum are 365 and 340 km respectively with the mean wavelength being quite close to that reported by Halliwell and Mooers (330 km). These results support the contention that an eigenmode representative of standing meanders does contain some propagating variance. Removing it affects estimates of both most energetic and mean wavelengths.

4. Propagation of meanders

a. Amplitude-dependent dispersion relation

Direct measurements of individual meanders are used to illustrate the dependence of the phase speed on wavelength as well as on amplitude. The component of the phase speed parallel to the long-term mean path was obtained for individual observations between 75° and 45°W. These data were then averaged onto a 50 km × 15 km grid in wavelength–amplitude space. The contoured results are presented in Fig. 6. The average error of the mean phase speed at each grid point is on the order of 1 km day^{-1}.

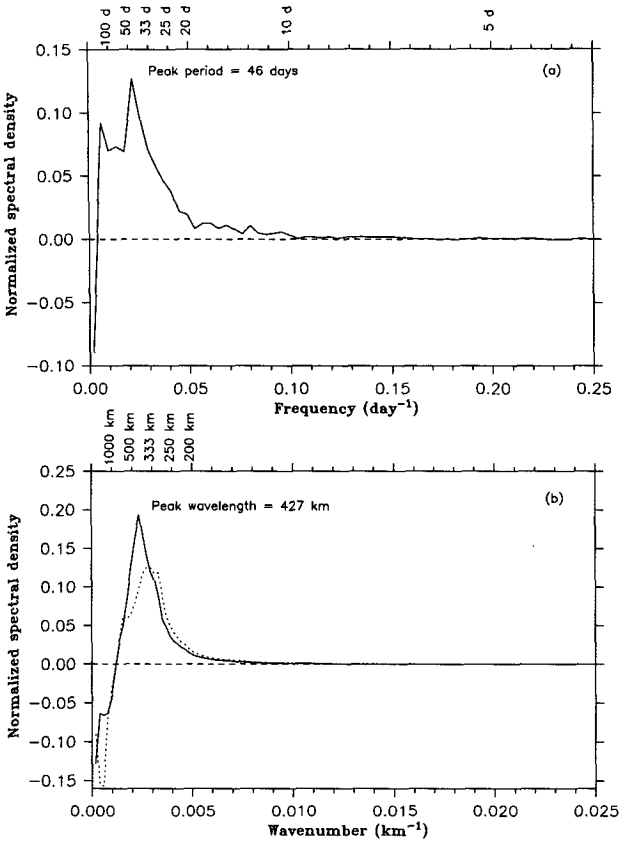

FIG. 4. Normalized propagating frequency (a) and wavenumber (b) spectra integrated from the propagating wavenumber–frequency spectrum. In the lower plot, the solid and dotted curves correspond to the data matrix with all modes and with the one without the second mode.

The phase speed generally decreases as the wavelength and/or amplitude increases. Such an amplitude dependence of the phase speed clearly demonstrates the amplitude dependence on propagation. Cushman-Roisin et al. (1993), using an equivalent-barotropic thin-jet model (a thin-jet model assumes that the width of the jet is much smaller than the length scale of alongstream variation and, hence, applies to meanders with wavelengths much larger than 50 km in this case), suggests that meander propagation is controlled by the downstream advection of meanders by the stream and the opposing retrogressive restoring effect, which consists of two mechanisms: the (planetary) β effect and vortex induction. In theory, effects of advection and β are independent of the wavelength and amplitude of meanders. Vortex induction, however, is stronger for longer waves in the linear limit (assuming infinitesimally small amplitudes). In the nonlinear context, for the same wavelength, vortex induction increased with meander amplitude. This nonlinear effect causes the phase speed to decrease as the amplitude increases for a given wavelength. Our observations are in qualitative agreement with these predictions.

The theory suggests that downstream advection is independent of the amplitude of meanders. However, the advection of meanders will be affected by the slope current to the north and recirculation to the south of the Gulf Stream, both of which flow in the direction opposite to the Gulf Stream. This effect may be insignificant for the upstream region where meander amplitudes are relatively small. However, as meander amplitude increases downstream, advection by the slope current and recirculation may tend to slow down the meander in addition to the enhanced vortex induction.

From Fig. 6, it is seen that meanders with wavelengths between 200 and 400 km and amplitudes on the order of 150 km have phase speeds close to zero. The average half-wavelength of these meanders, 150 km, is close to their amplitude. In other words, the average aspect ratio of crests and troughs of these near-stationary meanders is almost unity. That Gulf Stream rings are of very small ellipticity (nearly circular) and that their diameters at formation are similar to the half-wavelengths of these meanders (Brown et al. 1986) suggest that these meanders are the most probable ring-forming ones and that ring formation tends to occur

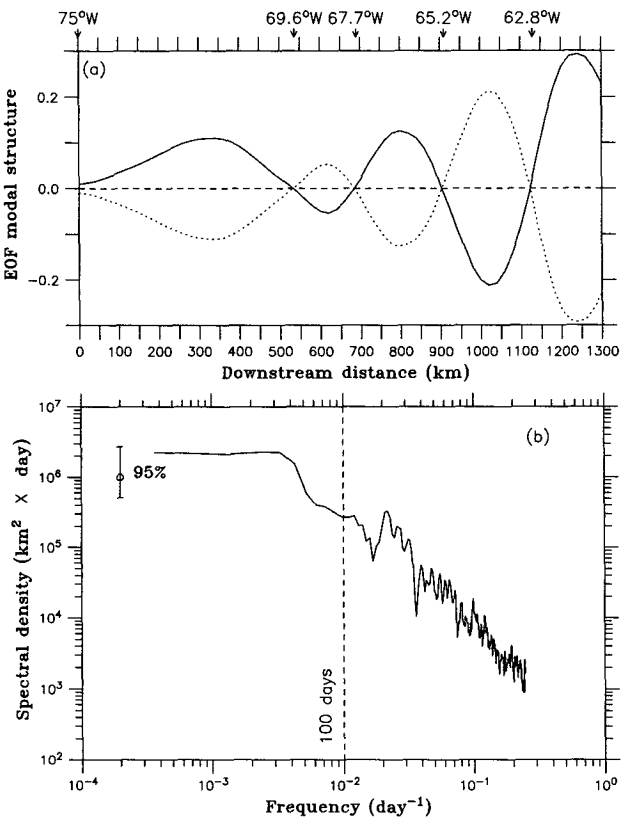

FIG. 5. The second EOF plotted antisymmetrically (a) and the frequency spectrum of the corresponding time series (b).

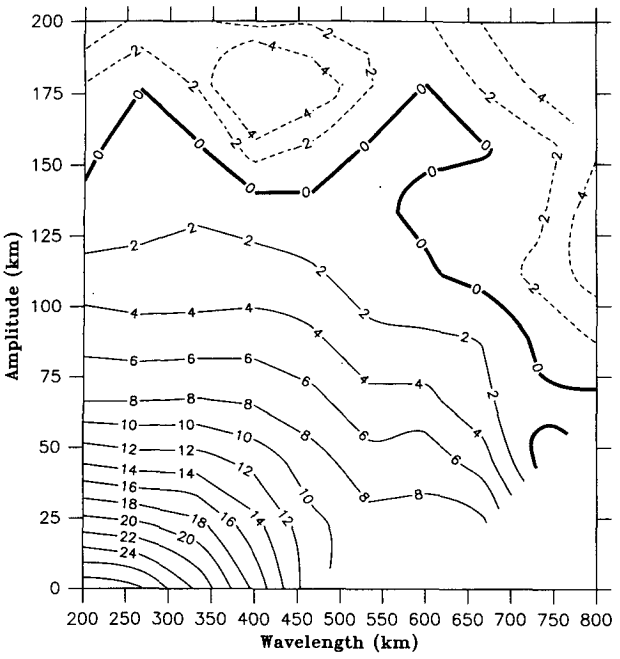

FIG. 6. The dependence of phase speed on wavelength and amplitude determined from individual measurements, presented as contours of phase speed in wavelength–amplitude space. The unit of the phase speed is km day^{-1}.

when the upstream restoring tendency of vortex induction and β equals that of downstream advection. When these meanders are very nearly stationary, their steep crests or troughs are more likely to be cut off from the stream by the downstream advection of the Gulf Stream working against the combined retrogressive effect of β, vortex induction, and upstream advection by the slope current (north of the stream) and recirculation (south of the stream).

The amplitude-dependent dispersion relation discussed above is based on measurements of meanders over a broad geographical range (75°–45°W). Figure 7 illustrates the longitudinal distribution of mean amplitude and phase speed averaged over 1-degree bins. It is seen that, from 75°–60°W (the region where spectral analysis is applied), the phase speed generally decreases while the amplitude increases. To examine whether this downstream decrease of mean phase speed is merely due to the finite-amplitude effect or associated with factors independent of amplitude, we employed a multiple linear regression $c = (S_A A + S_\lambda \lambda + S_X X)$ to individual observations between 75° and 60°W (where A, λ, and X are amplitude, wavelength, and longitudinal distance from 75°W, and the S are regression coefficients). Before the regression, the sample mean of each quantity was subtracted; each quantity is then normalized by the standard deviation so that magnitudes of the regression coefficients directly reflect the relative dependence of c on A, λ, and X. The resultant mean and 95% confidence interval of the coefficients are $(S_A, S_\lambda, S_X) = (-0.41 \pm 0.06, -0.21 \pm 0.06, -0.11 \pm 0.07)$. All coefficients are statistically smaller than zero, indicating that, apart from the decrease of phase speed as the wavelength or amplitude increases, meanders of the same wavelength and amplitude tend to travel more slowly the farther downstream they are found. Magnitudes of the coefficients indicate that the longitudinal dependence of phase speed is much weaker than the amplitude and wavelength dependence. We did not investigate factors responsible for this relatively small longitudinal dependence (e.g., change in water depth, stratification, stream transport, eddy influence, and topography, etc.).

The above regression analysis is only an attempt to evaluate the overall relative dependence of c on A, L, and X. One should note that the dependence of c on A changes with A (as seen from Fig. 6). For a fixed L, the dependence of c on A becomes stronger as A increases, consistent with the theoretical findings of Pratt (1988) and Cushman-Roisin et al. (1993).

Vazquez and Watts (1985) analyze Gulf Stream positions between 75° and 68°W obtained from IES and infrared images for a 3-year interval. They found that the phase speed of meanders having periods of 33 and 50 days decreases while the steepness (amplitude/wavelength) increases downstream. By inspecting Gulf Stream paths between 73° and 46°W derived from Geosat altimeter data, Kelly (1991) found that meanders have larger amplitudes and become less progressive in the eastern part of the region than they do in the upstream region. Those finding are qualitatively consistent with the dependence of phase speed on amplitude and geographical location observed in the present study.

b. Amplitude-averaged dispersion relation

We have presented an empirical amplitude-dependent dispersion relation based on direct measurements of individual meanders. However, the direct measurement algorithm cannot resolve meanders having wavelengths longer than about 800 km. In this section, propagation characteristics of meanders obtained from wavenumber–frequency spectra of path displacements between 75° and 60°W (section 3a) are used to derive an amplitude-averaged dispersion relation that extends to longer wavelengths; the sense of amplitude averaging comes from the fact that the spectral analysis takes into account meanders of all amplitudes.

The approach to obtain the dispersion relation from the propagating wavenumber–frequency spectrum is the same as that described in Lee and Cornillon (1996). The propagating and standing wavenumber spectra are obtained for each of a number of frequency bands by integrating the propagating and standing wavenumber–frequency spectra over the frequency band. The spectra are displayed in Fig. 8 for wavenumbers up to

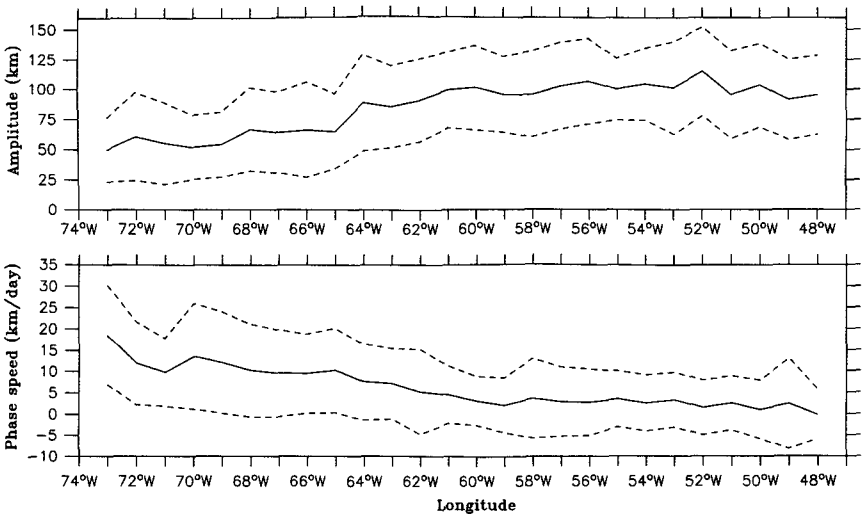

FIG. 7. Longitudinal variation of averaged amplitude (a) and phase speed (b) measured from individual meanders.

0.01 km^{-1} because the spectral density rolls off quickly to zero for wavenumbers larger than 0.01 km^{-1}. The positive ridge associated with progressive meanders is present at all periods. Retrogressive meanders indicated by the negative ridge exist at periods longer than 72 days. For those periods where progressive and retrogressive meanders coexist (i.e., longer than 72 days), the standing spectra have excess energy at a wavenumber between those of the positive and negative peaks in the propagating spectra. This energy reflects standing waves formed by oppositely traveling meanders of the same wavelength that result from the amplitude dependence of phase speed, as explained in detail in Lee and Cornillon (1996) through a kinematic argument. Phase speeds of progressive and retrogressive meanders are calculated from the center periods and wavelengths determined from the spectral peaks. For each period band, the spectrally derived wavelengths and phase speeds for different AR model orders (ranging from 6 to 24) are averaged. Lee (1994) found that the spectrally derived dispersion relation was consistent with the wavelength–phase speed relation determined from individual measurements (averaged over all amplitudes) and from CEOF analysis.

The resultant dispersion relation, denoted by triangles in Fig. 9, is compared with the one for the upstream region 74°–70°W (circles in Fig. 9) obtained in Lee and Cornillon (1996) using the same approach. Phase speeds of progressive meanders observed in the present study are generally smaller than those of the upstream region. This is attributed to the downstream increase in amplitude and the corresponding decrease in phase speed seen in Fig. 7.

The stationary wavelength of the larger domain, between 700 and 800 km, is smaller than that estimated for the upstream region, 1100 km. This is because meanders downstream of 70°W have larger amplitudes, and thus approach the zero phase speed at shorter wavelengths. The stationary wavelength for the region 70°–60°W, determined by analyzing the data for this region, is about 500 km. Therefore, the difference of stationary wavelengths between the large domain and the upstream region is also associated with the amplitude-dependent effect. In Lee and Cornillon (1996), it was shown that the wavelength of stationary meanders is close to that of standing meanders for the upstream region. A kinematic argument was used to explain that standing meanders were formed by near-stationary meanders of the same wavelength but different amplitudes. Given this scenario, we expect standing meanders downstream of 70°W to be shorter than those observed upstream by Lee and Cornillon (1996). From the spatial structure of the standing wave pattern shown by the second EOF presented in section 3 (Fig. 5), it is seen that the node-to-node distance of standing meanders is, in fact, much smaller downstream of 70°W (order 225 km yielding a wavelength on the order of 450 km, close to the 500 km value mentioned earlier) than it is upstream of that longitude, consistent with the decreasing stationary wavelength. Such a covariation of standing and stationary wavelengths further confirms the kinematic argument presented in Lee and Cornillon (1996).

The retrogressive phase speeds observed for the larger domain appear to be slightly smaller in magnitude than those observed in the upstream region. Given the relatively large uncertainty in the estimated phase speeds at these long wavelengths, this difference is not statistically significant.

From the above discussion, it is seen that a dispersion relation observed with data in the upstream region is not uniformly valid over a larger domain to

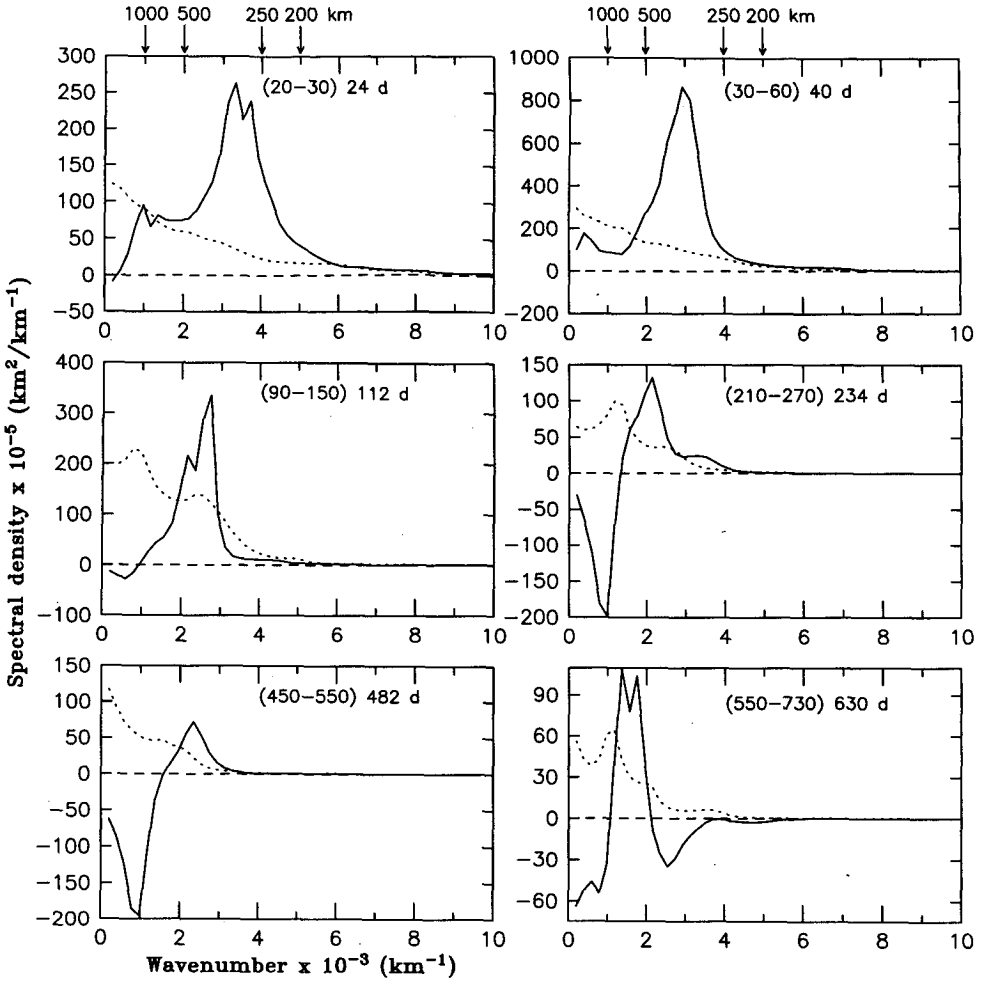

FIG. 8. Propagating and standing wavenumber spectra for various period bands derived from the propagating wavenumber–frequency spectrum presented in Fig. 2a. The period (band) is shown at the upper-right corner of each panel. Solid and dotted curves represent propagating and standing wavenumber spectra, respectively.

a large extent due to the increase in meander amplitude.

Relatively good agreement is found between the spectrally derived dispersion relation and that obtained by Halliwell and Mooers (1983) (stars in Fig. 9), which they determined graphically from their propagating wavenumber–frequency spectrum computed from data between 73° and 65°W. Retrogressive propagation, however, was not resolved in that study. Vazquez (1993) analyzed sea levels derived from the Geosat altimeter for a 2-year period for the region of 75°–60°W. He identified westward propagation at 5 km day^{-1} with a wavelength of 2000 km, which is not inconsistent with our estimated retrogressive phase speed at that wavelength.

The linear dispersion relation derived by Cushman-Roisin et al. (1993) is indicated by the solid curve in Fig. 9. The progressive phase speeds and the stationary wavelength observed for 75°–60°W are much smaller than the theoretical predictions. The fact that the theoretical relation is closer to the empirical relation for the upstream region and that the finite-amplitude effect is primarily responsible for differences between the smaller upstream region and the large domain suggests that nonlinearity needs to be considered to account for the effect of finite amplitude on meander propagation downstream of 70°W.

5. Growth of meanders

The evolution of Gulf Stream meanders is characterized by a signature of spatial and temporal growth: while the spatial envelope of meandering reflects the overall spatial growth, the evolution of the amplitude of individual meanders does not necessary follow the spatial envelope. This complicates the observational description and theoretical prediction of meander growth. In analytical and numerical models, the growth

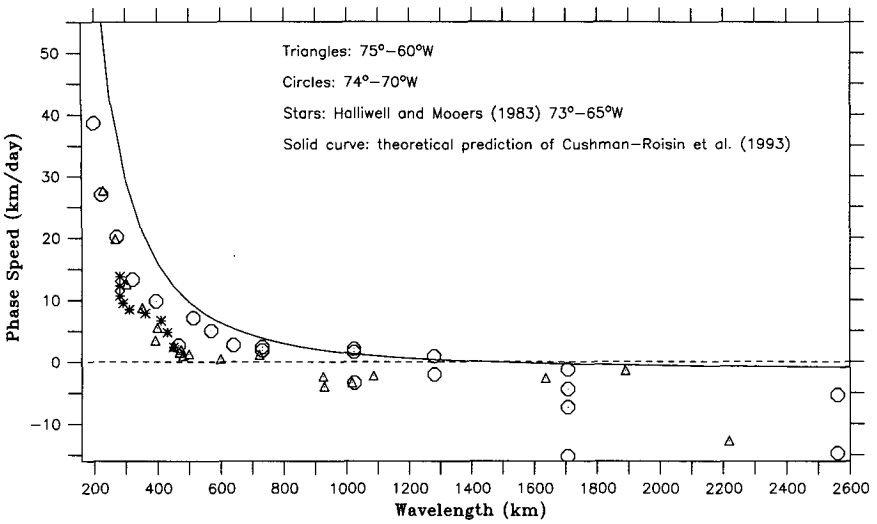

FIG. 9. Comparison of the spectrally derived dispersion relation for the region 75°–60°W (triangles) with that obtained for the region 74°–70°W in (circles), that determined by Halliwell and Mooers (1983) from their wavenumber–frequency spectrum (stars), and that theoretically predicted by Cushman-Roisin et al. (1993) (solid curve).

of unstable waves is reflected by the imaginary part of the complex wavenumber k and/or of the complex frequency ω for a wave of the form $e^{i(kx-\omega t)}$. One approximation is to treat k as real and ω complex. This results in a spatially periodic, temporally growing solution. The wave envelope is independent of x; that is, disturbances at different alongstream locations grow at the same rate. Most instability models developed for the Gulf Stream fall into this category (Orlanski 1969; Ikeda 1981; Johns 1988; Kontoyiannis 1992). A contrasting approach is to treat ω as real and k complex (Thacker 1976; Hogg 1976; Ikeda and Apel 1981). This leads to a temporally periodic and spatially growing solution. Disturbances are considered to originate at an upstream location. The spatial growth results in a downstream expanding wave envelope. The general case where both k and ω are complex is mathematically more difficult than taking k or ω to be real, and as a result, has not been used in instability models of the Gulf Stream. To date, the observational description of meander growth has been based on a spatial growth rate determined from the characteristics of meander amplitudes at different alongstream locations (Hansen 1970; Apel 1980; Watts and Johns 1982; Halliwell and Mooers 1979, 1983; Kontoyiannis and Watts 1994).

In this study, we provide two descriptions of the growth: 1) quantification of the spatial growth through the spatial structure of the amplitude of complex EOFs and 2) temporal growth through the amplitude evolution of individual meanders. Although the latter may not be totally independent of space, it avoids the assumption that growing disturbances only originate at an upstream location, and it provides a timescale of growth to compare with predictions of temporal growth models. Furthermore, the two types of observed growth rates may shed some light on the relation between temporal and spatial growth, which is theoretically undetermined for the case of the Gulf Stream. In the following, we first present the observed spatial and temporal growth rates from which the fastest-growing wavelength and period are determined and compared with model predictions. We then evaluate the relation between the two growth rates based on our observations taken in conjunction with previous theoretical studies.

The amplitude and phase of the leading CEOFs (first modes) for various bands of period are shown in Fig. 10. For periods shorter than 13 days, the CEOFs do not show a clear signature of progressive propagation. The CEOFs for periods longer than 174 days are dominated by combined signatures of standing and retrogressive meanders. For periods of 24–174 days, the general tilting of phase curves shows a dominance of progressive meanders. The spatial growth rate κ for each of the five periods from 24 to 174 days is obtained by fitting an exponential curve to the CEOF amplitude. These rates are plotted versus the period in Fig. 11a. Here κ at 24 and 40 days is associated with progressive meanders having wavelengths of 317 and 349 km (derived from a least square fit to the CEOF phase). However, we are unable to relate the spatial growth rates at 72, 112, and 174 days to a specific wavelength because they reflect the amplitude variation of both shorter progressive and longer standing meanders; hence, the derived wavelengths are very unreliable.

The largest spatial growth rate is found at 40 days (349 km) with $\kappa = 3.05(\pm 0.37) \times 10^{-3}$ km^{-1}. This is close to the growth rate reported by Halliwell and Mooers (1983), $3.2(\pm 1.3) \times 10^{-3}$ km^{-1} at a wave-

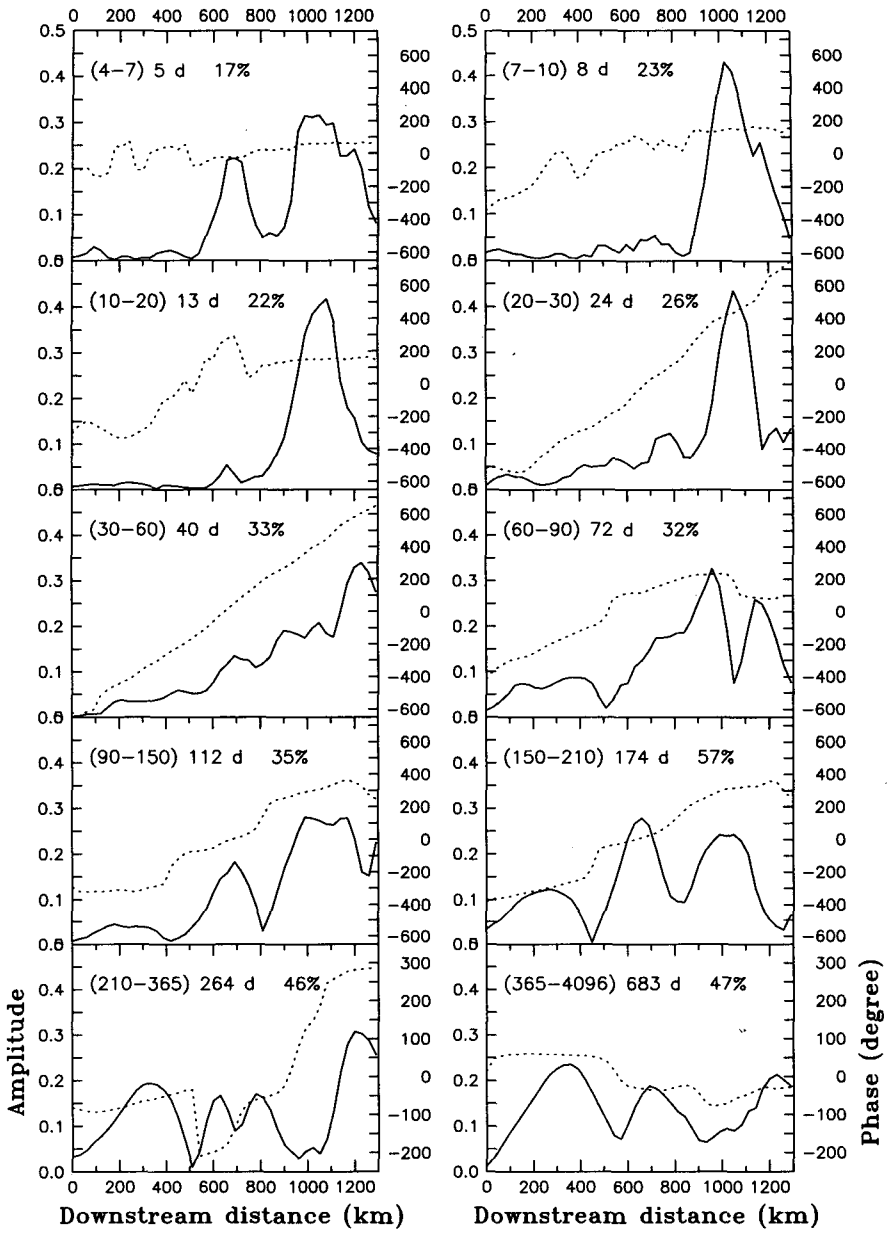

FIG. 10. The amplitude (solid curve) and phase (dotted curve) structures of complex empirical orthogonal functions (CEOFs) for various bands of periods.

length of 330 km, but larger than the rates observed by Apel (1980), 1.8×10^{-3} km^{-1} at 310 km, and Hansen (1970), $2(\pm 1) \times 10^{-3}$ km^{-1} at 300 km, both based on a very limited number of path realizations within a smaller geographical domain.

Based on CEOF analysis of IES data for the upstream region (74°–70°W), Kontoyiannis and Watts (1994) found a maximum κ of 4.2×10^{-3} km^{-1} at a period of 8 days. Analysis of the satellite data in the same region yields a maximum κ (3.4×10^{-3} km^{-1}) at 24 days, shorter than the 40 days observed in the larger domain but longer than the 8 days reported by Kontoyiannis and Watts. The satellite data of the upstream area analyzed using the same coordinate system, observational period, and analysis procedure as Kontoyiannis and Watts still yields a period for the maximum κ of 24 days. The difference in the period of the fastest-growing waves between the satellite and IES data could result from a depth dependence of short-period meander growth or from the limited capability of the satellite observation to resolve shorter-period meanders.

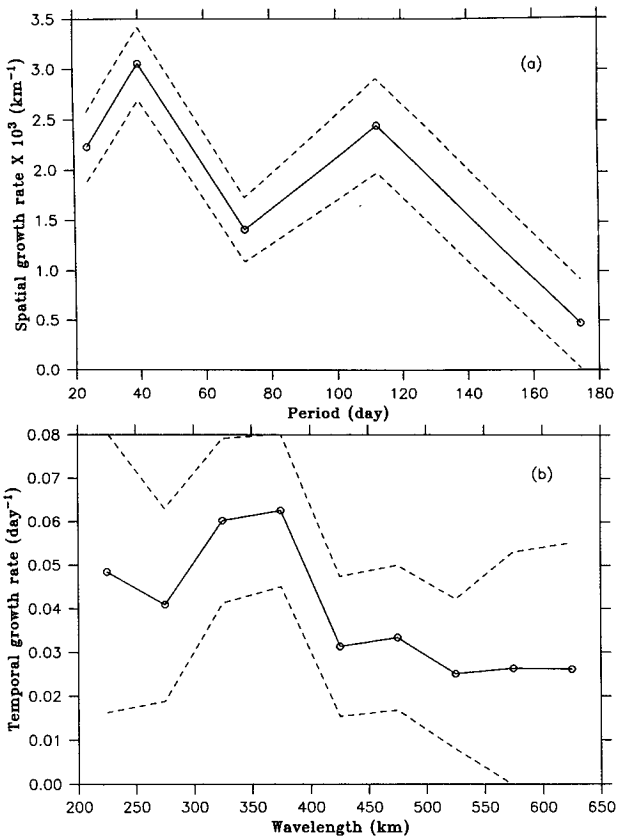

FIG. 11. The spatial growth rate vs period (a) and temporal growth rate vs wavelength (b). Dotted curves represent standard errors.

Temporal growth rates are quantified using individual observations of meanders with center locations falling in the region for which the CEOF analysis was performed (75°–60°W). For two measurements of the same meander observed at two consecutive times, t_1 and t_2, the temporal growth rate at time $t = (t_1 + t_2)/2$ is defined as $\sigma = 2/[A(t_1) + A(t_2)] \times [A(t_2) - A(t_1)]/[t_2 - t_1]$ (where A is the amplitude). The values of σ averaged over 50 km in wavelength are presented in Fig. 11b. The maximum σ occurs at wavelengths of approximately 350 km. The large errors (dashed curves in Fig. 11b) are caused both by the sensitivity to the measurement of amplitude (σ depends on the derivative of A) and by the poor exponential fit to A in time.

Using a two-layer linear baroclinic instability model with bottom topography, Orlanski (1969) predicted that, downstream of Cape Hatteras, the maximum temporal growth rate σ_{max}, 0.138 day^{-1}, occurs at a wavelength of 365 km and a period of 40 days, close to the wavelength and period where we found the maximum growth rate. Johns (1988), using a similar model but with realistic stratification, velocity profile, and potential vorticity distribution for 74°W, reported a σ_{max} of 0.08 day^{-1} at 390 km and 28 days. The Johns predictions of the wavelength and period of the maximum growth rate are consistent with our observations for the upstream area mentioned earlier, where the wavelength and period of the maximum spatial growth are 370 km and 24 days. Our observations and the model predictions suggest that instabilities tend to favor meanders having wavelengths on the order of 350 km and that there is a downstream increase in the period of maximum growth. Such an increase in period may be caused by several factors: 1) the downstream decrease in the phase speed of meanders having wavelengths of 350 km; 2) a downstream decrease of the bottom slope, as suggested by Orlanski (1969), and 3) a change in water depth. That the fastest-growing meanders (350 km) are somewhat shorter than the most energetic meanders (427 km) is consistent with the theoretical notion (Pedlosky 1981) that the most energetic wave realized at finite amplitude is longer than the linearly most unstable wave.

The observed σ_{max} (0.063 day^{-1}) is smaller than predictions by Orlanski (0.138 day^{-1}) and Johns (0.08 day^{-1}). The actual difference is not very significant because of the large uncertainty in our estimate of σ. However, it is important to highlight two differences between the observed and modeled σ. First, model predictions are initial growth rates of disturbances having infinitesimally small amplitudes. Ikeda (1981) shows that the growth rate of modeled meanders having a finite amplitude is smaller than the initial growth rate at the infinitesimal-amplitude stage, suggesting a nonlinear effect in meander growth. Although we do not have sufficient data to quantify the dependence of σ on amplitude, the average σ for meanders below the average amplitude, 0.089 day^{-1}, is indeed larger than that for meanders above the average amplitude, 0.022 day^{-1}, for the fastest-growing meanders (350 km). Second, linear predictions are for a "pure" exponential growth rate; the observed growth rates, however, are "net" ones resulting from growth as well as decay; hence, they would tend to be smaller.

In the literature, the comparison of observed spatial growth rate and modeled temporal growth rate was achieved by transforming one into the other through a velocity scale—for example, phase velocity in Watts and Johns (1982) and group velocity in Kontoyiannis and Watts (1994). The latter transformation is based on Gaster's (1962) finding that, for hydrodynamic instabilities, σ is related to κ through the group velocity c_g ($\sigma = \kappa c_g$). It is uncertain, however, whether or not the same relation holds in a geophysical context. Hogg (1976) argued that this relation is not valid for the recirculation region south of the Gulf Stream by demonstrating that spatially and temporally growing waves are separated by a neutral wave. Since our spatial and temporal growth rates are independently observed, they allow for an evaluation of the relation between the two. The ratio of σ/κ at the observed fastest-growing wavelength (350 km), 21 ± 6 km day^{-1}, is more than twice

the phase speeds at this wavelength, 8.7 km day^{-1} (Fig. 9). Therefore, the phase speed transformation is invalid. To evaluate the group velocity transformation, we use the relation $c_g = \partial f/\partial k$ (f and k are the frequency and wavenumber) to estimate the group velocity c_g for 350-km wavelength meanders from the spectrally derived dispersion relation based on the linear assumption. The resultant c_g, 31 km day^{-1}, is larger than σ/κ (21 km day^{-1}) by approximately 50%. A strict estimate of c_g for Gulf Stream meanders is troublesome because both c and c_g are functions of the amplitude as well as the wavelength. The amplitude dependence results in different c_g for the spectrally derived and directly measured dispersion relations at a wavelength of 350 km (Fig. 9). The value of c_g determined from the dispersion relation based on direct measurements is 26 km day^{-1}. This is still larger than, but closer to, σ/κ. Therefore, the group velocity transformation may be valid for dominant Gulf Stream meanders.

6. Differences between meander crests and troughs

Meander crests protrude to the north and meander troughs to the south of the mean Gulf Stream. The analysis of the propagation and growth of meanders presented thus far treats meander crests and troughs the same. Individual measurements of meander crests and troughs between 75° and 45°W allow for an analysis of the differences in geometric shape, the phase speed, and the growth rate between crests and troughs. Figure 12a presents the steepness of a meander crest or trough as a function of the length of the crest or trough (steepness is defined here as the ratio of amplitude to the length). For lengths shorter than 170 km, troughs are seen to be steeper than crests. In addition to this difference in geometric shape, troughs are found to travel more slowly than crests in general (Fig. 12b). Furthermore, the average temporal growth rate of troughs, 0.0671 ± 0.0199 day^{-1}, is larger than that of crests, 0.0317 ± 0.0149 day^{-1}. These features are consistent: larger growth rates result in larger steepness, and larger steepness implies larger amplitudes with smaller phase speed due to the amplitude-dependent effect. It is therefore the difference in growth rate that probably defines the other differences.

The asymmetry in the cross-stream structure of the Gulf Stream is likely to be partly, if not totally, responsible for the observed crest–trough differences. The horizontal velocity shear and the thermal gradient on the northern side of the stream are much larger than those on the southern side. Meacham (1988) modeled the consequence of an asymmetric jet on meander evolution using a two-layer contour dynamics model with multiple potential vorticity fronts that are asymmetrically distributed. He found that troughs tended to grow faster than crests as observed here. Pratt et al. (1992) also found that troughs steepened more readily than crests when the asymmetry in the cross-stream structure was taken into account in an equivalent-barotropic model.

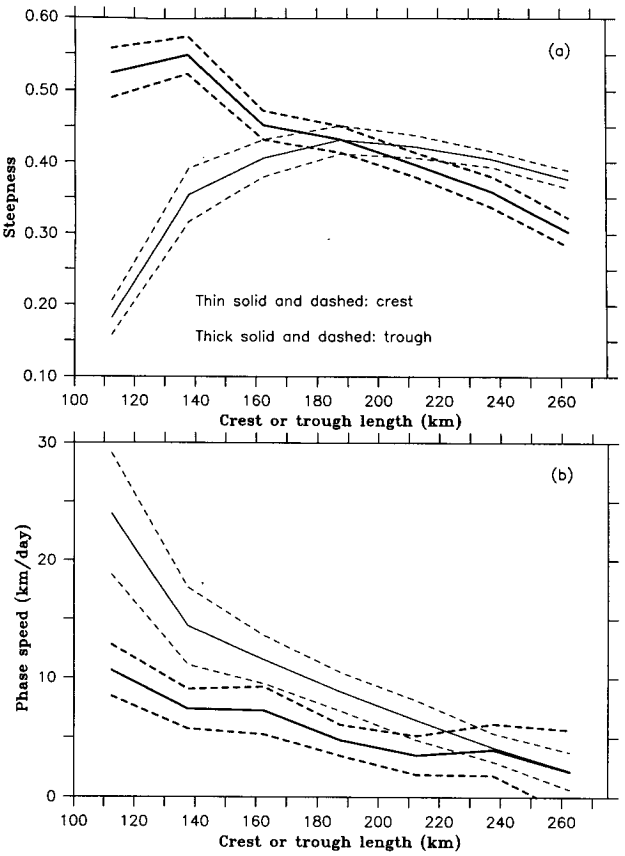

FIG. 12. Crest–trough difference of steepness (upper) and phase speed (lower). Dashed curves represent standard errors.

Apart from the skewed cross-stream velocity profile, topography may also play a role. Within the envelope of the Gulf Stream, the meridional bottom slope north of the mean path is slightly larger and water depth is smaller compared with the region south of the mean path. The effect of meridional change in bottom slope and water depth on meander growth is yet to be accessed.

Crest–trough differences in growth rate and steepness tend to imply that there could be more cold core rings forming from troughs than warm core rings forming from crests, unless troughs can sustain larger amplitudes at an equilibrium stage without pinching off as rings.

7. Effects of the New England Seamounts on meanders

Figure 13 shows the 93-month mean path of the stream and the one standard deviation envelope. The mean path begins to cross the New England Seamount Chain near 65.5°W. The envelope of the stream does

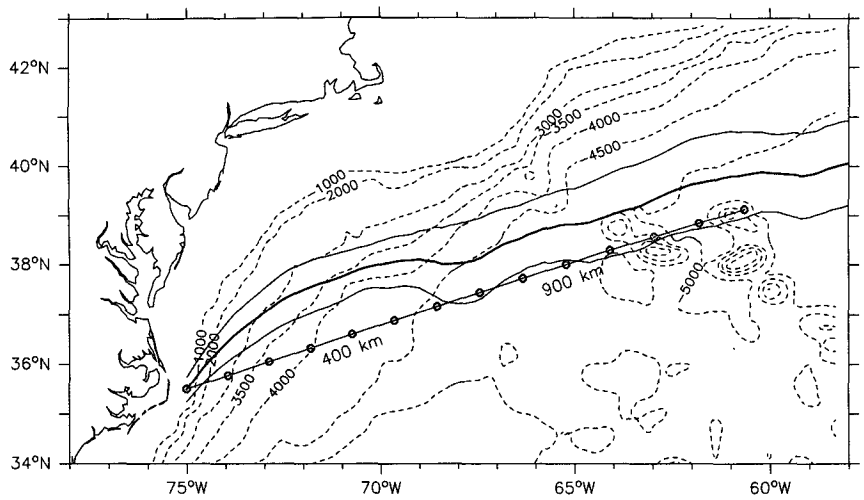

FIG. 13. The mean path (thick solid) and one standard deviation envelope (thin solid) of the Gulf Stream superimposed on isobaths (dashed). The mean path begins to cross the New England Seamount Chain near 65°W. The x axis is marked by the straight line; the distance between consecutive circles along the x axis is 100 km.

not expand significantly in this region. Figure 14 shows the spatial distribution of variance for frequency bands corresponding to periods <1 month, 1–2 months, 2–6 months, and >6 months. The approximate location at which the mean path begins to cross the seamounts is denoted by the vertical dashed line at 900 km (65.5°W). The variance of the 1–2 month band increases almost monotonically downstream across the seamount chain without abrupt change. All other bands (either shorter or longer periods) show local minima significant at the 95% confidence level immediately upstream of the seamounts.

It is noted that the 1–2 month band corresponds to dominant meanders (i.e., those having the most energetic period studied in section 3). The CEOFs shown in Fig. 10 further illustrate the features mentioned above. For periods shorter than the dominant band (40 days), there is a rapid increase in the amplitude over the seamount chain. For the most energetic band at the 40-day period, neither the phase nor the amplitude appear to be affected by the seamounts. For 264 and 683 days, the standing wave signature is significant, and the waves tend to show a node near 900 km (65.5°W) from the origin. It seems that these long-period standing me-

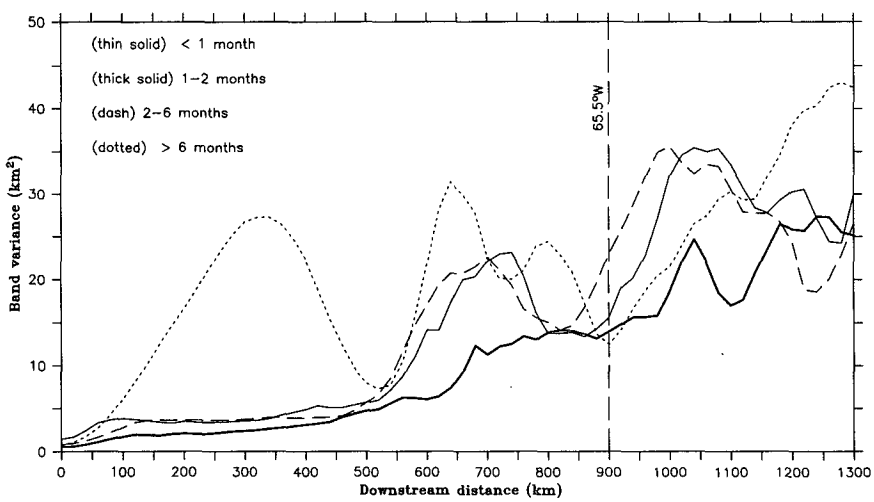

FIG. 14. Spatial distribution of variance for several period bands: <1 month (thin solid), 1–2 months (thick solid), 2–6 months (dashed), and >6 months (dotted). The location where the stream begins to cross the seamounts is shown by the dash line.

anders, which are relatively barotropic, are subject to the Taylor–Proudman constraint such that water columns tend not to move onto the seamounts north and south of the mean stream to avoid vortex squashing and stretching.

The local minimum in the variance of short-period meanders slightly west of 65.5°W is probably due to other mechanisms. Oey et al. (1992) suggest that a topographic bump (e.g., the Charleston bump) affects the current both downstream and upstream of the bump; the downstream influence is due to the development of downstream propagating meanders induced by the bump, while the upstream influence is associated with upstream propagating topographic Rossby waves excited at the bump. The southward intrusion of the isobaths near 65.5°W is similar to the Charleston bump except that the orientation is different. It is possible that it would also induce upstream and downstream effects in a way similar to that described by Oey et al. (1992), and thus result in excess variance to the east and west of 65.5°W.

These observations tend to explain why there has been confusion with regard to the effect of New England Seamounts in the past. The most energetic meanders are not affected by the seamounts. Studies attempting to quantify the influence of seamounts with gross meander characteristics such as envelope width see little effect because the gross statistics are dominated by the meanders of the most energetic period. Meanders having shorter or longer periods do, however, appear to be affected by the seamounts. Studies dealing with individual meanders not in the most energetic band will detect an effect. The mechanism through which the seamounts affect long-period meanders appears to be different from the way they affect short-period meanders. For long-period meanders, their lateral excursions tend to be constrained at the location where the mean path of the stream goes between two seamounts. For short-period meanders, the anomalously large variance before and over the seamount chain might be associated with upstream and downstream variabilities caused by the seamounts. Further study is needed to clarify these effects.

8. Concluding remarks

Analysis of the Gulf Stream path between 75° and 60°W indicates that the spectral signature of propagating and standing meanders is qualitatively similar to that observed in Lee and Cornillon (1996) for the upstream region, 74°–70°W. Progressive, retrogressive, and standing meanders coexist at periods of several months and longer. The most energetic propagating meanders for the region of 75°–60°W have a period of 46 days and a wavelength of 427 km. The latter is longer than previously thought (Halliwell and Mooers 1983).

An amplitude-dependent dispersion relation is obtained for the region of 75°–45°W. The dependence of phase speed on amplitude is found to be stronger than that on wavelength. The average phase speed decreases with downstream distance, primarily due to the downstream increase of meander amplitude. Consequently, a relation between phase speed and wavelength for the region west of 70°W, averaged over all amplitudes, is not uniformly valid for a larger domain. The wavelengths of both stationary and standing meanders are smaller downstream of 70°W compared with those upstream of this longitude. Such a covariation confirms the kinematic argument of Lee and Cornillon (1996) that standing meanders are formed by wave components of different amplitudes slowly traveling in opposite directions as a result of the finite-amplitude and β effects. The average stationary wavelength, 700–800 km for 75° and 60°W, is much shorter than that predicted by the linear dispersion relation of Cushman-Roisin et al. (1993).

The fastest-growing meanders have a period of approximately 40 days obtained for the region from 75° to 60°W and 24 days when only the upstream region (west of 70°W) is considered. The 40-day period is close to that of the most energetic meanders. The wavelength of the fastest-growing meanders, about 350 km, is shorter than the most energetic wavelength, 427 km. Such a difference in wavelength supports the theoretical notion that the most energetic waves with finite amplitudes are longer than the most unstable waves. Analysis of the relation between the spatial and temporal growth rates of the fastest-growing meanders indicates that these two quantities may be related by the group velocity.

Downstream propagating meander troughs are found to grow faster, and consequently are steeper and travel more slowly than meander crests. A possible explanation for these differences is the asymmetry in the cross-stream structure of the Gulf Stream.

The New England Seamounts do not have a significant effect on the most energetic meanders. However, meanders having periods either shorter or longer than the most energetic ones are affected by the seamounts. For long-period meanders, their lateral excursions seem to be constrained by the seamounts in order to conserve potential vorticity.

Acknowledgments. This research was performed with support from the Office of Naval Research (N00014-90-J-1564) and from the State of Rhode Island and Providence Plantations through salary support to P. Cornillon. All of the figures were generated using the interactive graphics package Plot Plus developed by Donald Denbo. The satellite data processing software used to process the images from which the surface fronts were digitized was developed by R. Evans, O. Brown, J. Brown, and A. Li of the University of Miami. Their continued support is greatly appreciated. Special thanks are due to Professor Randy Watts, Dr. Harris

Kontoyiannis, Dr. Larry Pratt, and Professor Benoit Cushman-Roisin for their valuable discussions.

REFERENCES

Auer, S. J., 1987: Five-year climatological survey of the Gulf Stream system and its associated rings. *J. Geophys, Res.*, **92,** 11 709–11 726.

Brown, O. B., P. Cornillon, S. R. Emmerson, and H. M. Carle, 1986: Gulf Stream warm rings: A statistical study of their behavior. *Deep-Sea Res.*, **33,** 1459–1473.

Cornillon, P., 1986: The effect of the New England Seamounts on Gulf Stream meandering as observed from satellite IR imagery. *J. Phys. Oceanogr.* **16,** 386–389.

——, and A. Boman, 1987: Meander propagation down stream of Cape Hatteras. *Eos. Trans. Amer. Geophys. Union,* **68,** pp. 341.

——, C. Gilman, L. Stramma, O. Brown, R. Evans, and J. Brown, 1987: Processing and analysis of large volumes of satellite-derived thermal infrared data. *J. Geophys. Res.*, **92,** 12 993–13 002.

——, T. Lee, and G. Fall, 1994: On the probability that a Gulf Stream meander crest detaches to form a warm core ring. *J. Phys. Oceanogr.*, **24,** 159–171.

Cushman-Roisin, B., L. J. Pratt, and E. Ralph, 1993: A general theory for equivalent barotropic thin jet. *J. Phys. Oceanogr.*, **23,** 91–103.

Gaster, M., 1962: A note on a relation between temporally increasing and spatial increasing disturbances in hydrodynamics stability. *J. Fluid Mech.*, **14,** 222–224.

Gilman, C. S., 1988: A study of the Gulf Stream downstream of Cape Hatteras 1975–1986. M.S. thesis, Graduate School of Oceanography, University of Rhode Island, 75 pp.

Halliwell, G. R., Jr., and C. N. K. Mooers, 1979: The space–time structure and variability of the shelf water–slope water and Gulf Stream surface temperature fronts and associated warm-core eddies. *J. Geophys. Res.*, **84,** 7707–7725.

——, and ——, 1983: Meanders of the Gulf Stream downstream from Cape Hatteras. *J. Phys. Oceanogr.*, **13,** 1275–1292.

Hansen, D. V., 1970: Gulf Stream meanders between Cape Hatteras and Grand Banks. *Deep-Sea Res.*, **17,** 495–511.

——, and G. A. Maul, 1970: A note on the use of sea surface temperature for observing ocean currents. *Remote Sens. Environ.*, **1,** 161–164.

Hogg, N. G., 1976: On spatially growing baroclinic waves in the ocean. *J. Fluid Mech.*, **78,** 217–235.

Ikeda, M., 1981: Mesoscale eddies of a strong eastward flowing jet using a two-layer quasi-geostrophic model. *J. Phys. Oceanogr.*, **11,** 526–540.

——, and J. R. Apel, 1981: Mesoscale eddies detached from spatially growing meanders in an eastward oceanic jet using a two-layer quasi-geostrophic model. *J. Phys. Oceanogr.*, **11,** 1638–1661.

Johns, W. E., 1988: One-dimensional baroclinically unstable waves on the Gulf Stream potential vorticity gradient near Cape Hatteras. *Dyn. Atmos. Oceans,* **11,** 323–350.

Kelly, K. A., 1991: The meandering Gulf Stream as seen by the Geosat altimeter: Surface transport, position, and velocity variance from 73° to 46°W. *J. Geophys. Res.*, **96,** 16 721–16 738.

Kontoyiannis, H., 1992: Variability of the Gulf Stream path between 74°W and 70°W: Observations and quasi-geostrophic modeling of mixed instabilities. Ph.D. dissertation, Graduate School of Oceanography, University of Rhode Island, 137 pp.

——, and D. R. Watts, 1994: Observations on the variability of the Gulf Stream path between 74° and 70°W. *J. Phys. Oceanogr.*, **24,** 1999–2013.

Lee, T., 1994: Variability of the Gulf Stream path observed from satellite infrared images. Ph.D. dissertation, Graduate School of Oceanography, University of Rhode Island, 188 pp.

——, and P. Cornillon, 1995: Temporal variation of meandering intensity and domain-wide lateral oscillations of the Gulf Stream. *J. Geophys. Res.*, **100,** 13 603–13 613.

——, and ——, 1996: Propagation of Gulf Stream meanders between 74° and 70°W. *J. Phys. Oceanogr.*, **26,** 205–224.

Maul, G. A., P. W. Witt, A. Yanaway, and S. R. Baig, 1978: Geostationary satellite observations of Gulf Stream meanders: Infrared measurements and time series analysis. *J. Geophys. Res.*, **83,** 6123–6135.

Meacham, S. P., 1991: Meander evolution on piecewise-uniform, quasi-geostrophic jets. *J. Phys. Oceanogr.*, **21,** 1139–1170.

Oey, L.-Y., T. Ezer, G. L. Mellor, and P. Chen, 1992: A model study of "bump" induced western boundary current variabilities. *J. Mar. Sys.*, **3,** 321–342.

Orlanski, I., 1969: The influence of bottom topography on the stability of jets in a baroclinic fluid. *J. Atmos. Sci.*, **26,** 1216–1232.

Pedlosky, J., 1981: The nonlinear dynamics of baroclinic wave ensembles. *J. Fluid Mech.*, **102,** 169–209.

Pratt, L. J., 1988: Meandering and eddy detachment according to a simple (looking) path equation. *J. Phys. Oceanogr.*, **18,** 1627–1640.

——, J. Earles, P. Cornillon, and J.-F. Cayula, 1992: The nonlinear behavior of varicose disturbances in a simple model of the Gulf Stream. *Deep-Sea Res.*, **38**(Suppl.), 591–622.

Richardson, P. L., 1981: Gulf Stream trajectories measured with free drifting buoys. *J. Phys. Oceonogr.*, **11,** 999–1010.

Robinson, A. R., J. R. Luyten, and F. C. Fuglister, 1974: Transient Gulf Stream meandering. Part I: An observational experiment. *J. Phys. Oceanogr.*, **4,** 237–255.

Teague, W. J., and Z. R. Hallock, 1990: Gulf Stream path analysis near the New England Seamounts. *J. Geophys. Res.*, **95,** 1647–1662.

Thacker, W. C., 1976: Spatial growth of Gulf Stream meanders. *Geophys. Astrophys. Fluid Dyn.*, **7,** 271–295.

Vazquez, J., 1993: Observations on the long-period variability of the Gulf Stream downstream of Cape Hatteras. *J. Geophys. Res.*, **98,** 20 133–20 147.

——, and D. R. Watts, 1985: Observations on the propagation, growth, and predictability of Gulf Stream meanders. *J. Geophys. Res.*, **90,** 7143–7151.

Watts, D. R., and W. E. Johns, 1982: Gulf Stream meanders: Observations on propagation and growth. *J. Geophys. Res.*, **87,** 9467–9476.